ELECTRONIC STRUCTURE AND MÖSSBAUER ISOMER SHIFT OF THE IRON ATOM ISOLATED IN CRYSTALLINE ARGON MATRIX

M. BRAGA, A.R. RIEGO AND J. DANON

CENTRO BRASILEIRO DE PESQUISAS FISICAS - CBPF -

RIO DE JANEIRO - BRASIL

ABSTRACT

Multiple Scattering calculations were performed on an $FeAr_{12}$ cluster in order to describe the iron atom trapped in a crystalline argon matrix. The total electron densities at the iron nucleus derived from these calculations are used to interpret Mössbauer Isomer Shift data. The different bonding mechanisms contributing to the metal atom-rare gas matrix interaction are also investigated. It is found the overlap distorsion effect of the metal wave functions to play a major role in the calculated electron densities. The iron isomer shift calibration constant was found to be -0.22 a_o^3 mm sec^{-1}.

I. INTRODUCTION

Hyperfine interactions between the nuclear and the electronic energy levels as studied by Mössbauer spectroscopy are known to provide valuable information about the electronic structure and chemical bonding in a wide variety of both inorganic and organic compounds. The Mössbauer Isomer Shift (IS) gives a direct measure of the total electron density at the nuclear site. In a non-relativistic approximation, the IS energy shift can be written as:

$$\Delta E_{IS} = \frac{2}{3}\pi e^2 Z \Delta\langle r^2\rangle \Delta\rho(0) \qquad (1)$$

$$\Delta\rho(0) = \psi_A^2(0) - \psi_S^2(0) \qquad (2)$$

where $\psi_A^2(0)$ and $\psi_S^2(0)$ are the total electron densities at the absorber and source nuclei, respectively and $\Delta\langle r^2\rangle = \langle r^2\rangle_e - \langle r^2\rangle_g$ is the change in nuclear mean square radius between excited and ground state. For a given nucleus, all factors are constant except the electron density difference term $\Delta\rho(0)$. Eq. (1) may be rewritten as:

$$\alpha = \Delta E_{IS}/\Delta\rho(0) \qquad (3)$$

where α is the IS calibration constant and contains only nuclear factors. However, an accurate determination of this constant from nuclear theory has not proved feasible. Instead, it must be determinated from measured IS and calculated charge densities for the nucleus in two different chemical environments. For the iron IS calibration constant the values are at great variance, ranging from -0.1 to -0.7 a_o^3 mm sec^{-1} (1).

The interpretation of the IS data has ussually been given in terms of free atom or free ion models[2]. In order to account for the influence of the neighboring atoms, the free atom or free ion wave-functions are modified to include covalency and overlap effects[3-5]. More recently, Molecular Orbital wave functions obtained from ab-initio[1,6], Multiple Scattering[7] or semi-empirical[8] calculations have also been used.

The use of the rare-gas matrix isolation technique to solve the problem of the iron IS calibration was suggested by Jaccarino and Wertheim[9]. In such systems, free atom or free ion functions should be a reasonable approximation to the true wave functions of the trapped atom. The first successful result of a Mössbauer experiment with ^{57}Fe atoms isolated in argon matrix was reported by Barrett and McNab[10]. Shortly after the Mössbauer spectra of ^{57}Fe was measured in argon, krypton and xenon[11]. These spectra showed and absorption line with an IS of -0.75 ± 0.03 mm sec^{-1} with respect to an iron foil at 300K. In adition, $^{57}Fe^{+}$ ions isolated in xenon matrix with $3d^{6}4s^{1}$ [12] and $3d^{7}$ [13] configuration have also been studied. Iron atoms in N_2[14], CH_4 and CO_2[15] matrices showed the same IS as in the case of the rare-gas matrices. Thus experiments in non-rare-gas inert matrices support the concept of an almost free isolated atom, i. e. the influence of the matrix itself can be neglected.

However, optical spectra indicate an appreciable amount of interaction between the trapped atom (mainly in the case of transition metal atoms) and the matrix. The matrix perturbation on the atomic levels can be as great as 3000 cm^{-1} [16]. There is also marked level splitting due to a non-cubic symmetry at the impurity site(vacancies or another metal atom as one of the nearest neighbors[11]) or the presence of the metal atom in two different crystallographic si-

te.

The contribution of the overlap distorsion effect to the measured IS in rare gas matrices have been analised by several authors[17,18]. The overlap between the metal and ligand wavefunctions was included by orthogonalizing the s-metal functions to suitable combinations of ligand s and p orbitals transforming under a_{1g} symmetry, the ligand-ligand overlap being neglected. The modification of the atomic wave functions by the crystalline potential (covalent effect) have also been investigated[18].

However, a deeper understanding of the different bonding mechanisms involved in trapped atom-host lattice interaction should require to include simultaneously all the effects above mentioned. It is well known that band theory in its conventional form cannot be applied to the description of localized states in solids. The application of the Molecular Orbital theory is based on the assumption that a representative small cluster of atoms (usually the trapped atom and its nearest neighbors) provides a suitable representation of the electronic environment at the impurity site in the crystal. The Discrete Variational Method is conection with the Cluster model has been employed by Walch and Ellis to study the IS of the iron atom in argon matrix[18]. However, the calculation was not converged to self-consistency and the calculated electron density is probably uncertain by 30%[19]. Combining the calculated $\Delta\rho(0)$ with the FeF_2 IS[11] (where the iron configuration is very close to $3d^6 4s^0$) gives $\alpha = -0.38\ a_o^3$ mm sec^{-1}[1].

The Multiple Scattering method has been widely applied to the study of both perfect and locally perturbed solids[20]. In a recent communication[21] it has been used to describe the electronic structure

and related properties of the hydrogen impurity in crystalline argon matrix. It has been shown that the main features of the bulk electronic structure and of the locally perturbed argon matrix are adequatelly reproduced by the Multiple Scattering Cluster Model.

In the present work we have carried out Multiple Scattering calculations for the iron atom isolated in crystalline argon matrix. Calculated wave functions are used to get the electron densities at the iron nucleus. These are correlated to the Mössbauer IS and interpreted in terms of the different bonding mechanisms involved in the metal-host lattice interaction. The IS calibration constant have also been evaluated.

II. COMPUTATIONAL METHOD

The Spin-polarized Multiple Scattering method[22] in its muffin-tin form with Slater's Xα local exchange have been applied to a cluster consisting of an iron atom and its twelve nearest neighbor argon atoms. This cluster was designed to represent the iron impurity substitutionally placed on an argon site in the fcc crystal. The Ar-Ar distance was assumed to be that of bulk crystalline argon. It has been further assumed the Fe-Ar distance to be the same as the Ar-Ar distance. The values of the α parameter for the exchange potential inside the Fe and Ar spheres were those calculated by Schwarz[23]. In the intersphere and outer region a weighted average of the atomic values was used.

Calculations have been carried out with three different initial iron configurations: $3d^6 4s^2$, $3d^7 4s^1$ and $3d^6 4s^{1+}$. All the calculations were carried to self-consistency all the electrons (core+valence) included in each SCF cycle.

The Multiple Scattering method have been described in detail in a number of papers[22]. By using the muffin-tin approximation for the molecular potential, the wave functions may be calculated numerically without the use of basis sets. In each muffin-tin sphere i the orbitals are given by:

$$\phi(r) = \sum_{\ell m} C^{i}_{\ell m} R_{\ell}(r) Y_{\ell m}(\theta,\phi) \qquad (4)$$

where $Y_{\ell m}(\theta,\phi)$ are the spherical harmonic functions. In the Fe and outer region we are using $\ell=0$ and $\ell=4$ for orbitals of a_{1g} symmetry, $\ell=2$ and $\ell=4$ for e_g and t_{2g}, $\ell=4$ for t_{1g}, $\ell=3$ for a_{2u} and t_{2u} and $\ell=1$ and $\ell=3$ for t_{1u}. In the ligand spheres we are using up to $\ell=1$.

In the interatomic region, the wave function is expanded in terms of spherical Bessel and Hankel functions. Eigenvalues and eigenvectors are obtained by the condition that the orbitals and their derivatives should be continuous across the sphere boundaries. In the case of the charged $FeAr_{12}^{+}$ cluster, a Watson sphere with charge -1 was used.

III. ORBITALS AND ORBITAL ENERGIES

The calculated energy spectra for the $Fe(3d^6 4s^2)Ar_{12}$, $Fe(3d^7 4s^1)Ar_{12}$ and $Fe(3d^6 4s^1)Ar_{12}^+$ clusters are given in fig 1-3. The terms inside the brackets indicate the iron configuration assumed at the beginning of each calculation. The energy labels are labeled according to the irreducible representations of the cubic symmetry group O_h. For comparision purposes, the energy spectrum of the $ArAr_{12}$ cluster[21] is also included in fig. 1.

Insert figures 1, 2, 3

We shall briefly discuss the main features arising from the cluster calculation of the argon crystalline bulk. For the argon crystal, many energy band calculations have been reported[24] and the comparision of the direct band gap and valence band widths to the experimental optical properties have been the usual criteria to test the accuracy of a given calculation. The energy difference between the HOMO (t_{1g}) and LUMO (a_{1g}) is found to be 0.68 Ry, which is in good agreement with the crystal band gap obtained from band calculations using the Xα exchange approximation[24]. However, it differs from the experimental value (1.04 Ry) and also from band calculations using the Hartree-Fock exchange. Virtual levels calculated in the Xα model do not, in the case of the Van der Waals solid, correspond to the physical conduction levels[24]. Thus results are more reliable when relate to bulk ground state properties. The band width of the 3s and 3p band are 0.047 and 0.079 Ry, respectively, in reasonable agreement with previous results from band calculations[24].

The argon bulk electronic structure is not substantially modified after replacing the central argon atom by an iron atom. The net effect is the remotion of the a_{1g} and t_{1u} levels localized on the central argon atom from the 3s and 3p band respectively and the appearance of the Fe 3d, 4s and 4p(unoccupied) valence levels in the crystal fundamental gap. In the case of the $Fe(3d^6 4s^1)Ar_{12}^+$ cluster the e_g and t_{2g} spin up iron 3d levels fall inside the Ar 3p band. The small changes in the argon bulk electronic structure are mainly due to the spin polarization effects produced by the unpaired 3d electrons of the iron atom. Polarization of the ligand atoms by the metal will in turn increase the crystalline potential. However this effect is very small and completely overcome by the much stronger overlap distorsion effect (see section IV). The impurity levels are highly localized on the metal atom and do not mix with the the ligand wave functions to any significant extent. In Table I we are giving the charge distributions in the different muffin-tin regions of the $ArAr_{12}$ and $FeAr_{12}$ clusters. Only a very small

Insert Table I

fraction of the total number of electrons is in the interatomic and outer region. Thus the muffin-tin approximation seems to be a realistic approximation to the true crystal potential. On the other hand, the charge in the argon sphere remains unchanged when going from the argon to the iron clusters. In the $Fe(3d^6 4s^1)Ar_{12}^+$ case all the iron electrons are inside the muffin-tin sphere. In the other cases, some of the 4s charge is in the intersphere region.
Table II gives the energies and charge distribution for orbitals

of a_{1g}, e_g and t_{2g} symmetry for the $Fe(3d^6 4s^2)Ar_{12}$ cluster. The

Insert Table II

$3a_{1g}$, $4e_g$ and $4t_{2g}$ are almost pure 4s and 3d iron levels without any significant ligand admixture. In the case of $Fe(3d^7 4s^1)Ar_{12}$ the situation is completely similar. In the $Fe(3d^6 4s^1)Ar_{12}^+$ the $2a_{1g}$ spin up level has a slightly iron 4s component (about 12% of an electron) and as result of this interaction it is lowered in energy (see fig. 3). From data in tables I and II we can concluded the marked atomic-like character of the iron and argon atoms, i.e. covalent effects in the trapped atom-rare gas matrix are almost negligible.

IV. ELECTRON DENSITIES AT THE IRON NUCLEUS AND THE ISOMER SHIFT CALIBRATION CONSTANT

In Table III we are giving the total electron density at the iron nucleus and the contributions from the different a_{1g} orbitals for the $FeAr_{12}$ clusters and the free iron atom. For the

Insert figure III

$Fe(3d^6 4s^2)Ar_{12}$ cluster we obtain $\Delta\rho(0) = +1.77$ a.u. relative to the free atom. Our result is in disagreement with the value previously reported by Walch and Ellis (-0.94). However a positive $\Delta\rho(0)$ for the trapped iron relative to the free atom can be explained by two different mechanisms: the contraction of the radial part of the iron 4s orbitals which leads to an increased 4s electron density at the nucleus and the contribution from the Ar 3p orbital transforming under a_{1g} symmetry. The inner Fe orbitals are not substantially modified.

Different bonding mechanisms can be regarded as contributing to the metal atom-rare gas lattice interaction. According to Adrian[25] the effect of a rare-gas matrix upon a trapped atom may be divided in three different parts: the attractive, Van der Waals interaction, the repulsive interaction and the overlap distorsion effect. In the following we shall discuss the relative importance of these interactions in determining the calculated electron densities at the iron nucleus.

The first two effects may be identified with the 6 and 12 terms of the "6-12" Lennard-Jones potential, respectively. The net effect is a slight expansion of the wave functions of the interacting species, i.e. the mean atomic radius is increased slightly. Such an expansion of the atomic wave functions(in the case of the iron atom,

the 4s functions are the most affected) will tend to reduce the electron density at the iron nucleus. The net effect of the Van der Waals interaction is therefore a negative contribution to $\Delta\rho(0)$.

The overlap distorsion effect can be described as a shrinking of both the metal and ligand orbitals having the same spin in order to reduce the forbidden overlap between them. The consequence is a repulsive interaction energy between the atoms involved, which tends to push charge on the nucleus of the atomic species involved. It is clear that the net result of this interaction will be to increase the electron density at the nuclear site. For the $FeAr_{12}$ clusters (with the exception of the $Fe(3d^74s^1)Ar_{12}$ cluster) the contraction of the 4s iron orbitals is the main positive contribution to the calculated $\Delta\rho(0)$. Figure 4 shows this effect for the $3a_{1g}$ spin up orbital (Fe 4s). The other iron orbitals are not

Insert figure 4

significatively modified. In the case of the $Fe(3d^74s^1)Ar_{12}$ the increased 3d population leads to an increased shielding of the nuclear charge which in turn produce a marked expansion of the 3s and 4s iron functions. This shielding effect is much stronger than the overlap distortion and as a consequence the 4s contribution to the total electron density is considerably lowered compared to the free atom (see Table III).

The calculated electron density for the $Fe(3d^64s^2)Ar_{12}$ cluster gives one point of the two required for the IS calibration constant. For the other, we shall use FeF_2 and assume[1,11] that the iron configuration corresponds to the free ion Fe^{+2} $3d^64s^0$. The IS of

the FeF_2 is 1.57±0.01 mm sec^{-1} relative to the iron at 300K. For the FeF_2 electron density we have used that of the Fe^{+2} $3d^6 4s^0$ free ion obtained from an atomic Xα calculation. We obtain the iron IS calibration constant to be -0.22 a_o^3 mm sec^{-1}. This values is in good agreement with recent ab-initio calculations[1,6]. It is interesting to observe that these elaborate methods of calculating wave functions confirm the previous value obtained by the use of Pauling's model of the chemical bond[4].

REFERENCES

1. K. J. Duff, Phys. Rev. B9, 66(1974).

2. see, for example, Chemical Applications of Mössbauer Spectroscopy, edited by V. I. Goldanskii and R. H. Herber(Academic, New York, 1968); The Mössbauer Effect and its Applications in Chemistry, Advances in Chemistry Series 68, edited by R. F. Gould(American Chemical Society, Washington, 1967).

3. E. Simānek and Z. Sroubek, Phys. Rev. 163, 275(1967); E. Simānek and A. Y. C. Wong, Phys. Rev. 166, 348(1968).

4. J. Danon in IAEA Panel on the Applications of the Mössbauer Effect in Chemistry and Solid State Physics, p. 89, International Atomic Energy Agency, Vienna, 1966.

5. L. R. Walker, G. K. Wertheim and V. Jaccarino, Phys. Rev. Letters 6, 98(1961).

6. P. S. Bagus, U. I. Walgren and J. Almlof, J. Chem. Phys. 64, 2324 (1976); W. C. Nieuwpoort, D. Post and P. Th. VanDuijnen, Phys. Rev B17, 91(1978).

7. M. L. de Siqueira, S. Larsson and J. W. D. Connolly, J. Phys. Chem. Solids 36, 1419(1975); D. Guenzburger, B. Maffeo and M. L. de Siqueira, J. Chem. Phys. Solids 38, 35(1977); D. Guenzburger, D. M. S. Esquivel and J. Danon, Phys. Rev. B18, 4561(1978).

8. A. Trautwein, F. E. Harris, A. J. Freeman and J. P. Desclaux, Phys. Rev, B11, 4101(1975); A. Trautwein and F. E. Harris, Phys. Rev. B7, 4755(1973); A. Trautwein and F. E. Harris, Theoret. Chim. Acta 30, 45(1973).

9. V. Jaccarino and G. K. Wertheim in Proceedings of the Second International Conference on the Mössbauer Effect, Saclay, France, 1961, edited by D. M. J. Compton and A. H. Schoen, p. 260 (wiley, New

York, 1962).

10. P. H. Barrett and T. K. McNab, Phys. Rev. Letters 25, 1601(1970).
11. T. K. McNab, H. Micklitz and P. H. Barrett, Phys. Rev. B4, 3787 (1971).
12. H. Micklitz and F. J. Litterst, Phys. Rev. Letters 33, 480(1974).
13. H. Micklitz and P. H. Barrett, Phys. Rev. Letters, 28, 1547(1972).
14. H. Micklitz, P.H. Barrett, Appl. Phys. Letters 20, 387(1972).
15. C. Klee, T. K. McNab, F. J. Litterst and H. Micklitz, Z. Physik 270, 31(1974).
16. D. M. Mann and P. H. Broida, J. Chem. Phys.55, 84(1971).
17. T. K. McNab, H. Micklitz and P. H. Barrett in Mössbauer Isomer Shifts, edited by G. K. Shenoy and F. E. Wagner, p. 225 (North-Holland, 1978).
18. P. F. Walch and D. E. Ellis, Phys. Rev. B7, 903(1973).
19. A. J. Freeman and D. E. Ellis in Mössbauer Isomer Shifts, p. 113.
20. see, for example, K. H. Johnson, Ann. Rev. Phys. Chem. 26, 39(1975).
21. A. R. Riego, J. R. Leite and M. L. de Siqueira, Sol. State Comm. 31, 25(1979).
22. K. H. Johnson, J. Chem. Phys. 45, 3085(1966); Adv. Quantum Chem. 7, 143(1973).
23. K. Schwarz, Phys. Rev. B5, 2466(1972).
24. S. B. Trickey, F. R. Green Jr. and F. W. Averill, Phys. Rev. B8, 4822(1973) and references therein.
25. F. J. Adrian, J. Chem. Phys.32, 972(1960).

TABLE I

Total charge distributions in muffin-tin regions for $ArAr_{12}$ and $FeAr_{12}$ clusters.

	CENTRAL ATOM	ARGON ATOM	INTERATOMIC REGION	OUTER SPHERE
$ArAr_{12}$	17.89	17.87	1.69	0.02
$Fe(3d^6 4s^2)Ar_{12}$	25.59	17.88	1.80	0.10
$Fe(3d^6 4s^1)Ar_{12}^+$	25.00	17.87	1.54	0.08
$Fe(3d^7 4s^1)Ar_{12}$	25.70	17.87	1.73	0.10

TABLE II

Orbital energies and Integrated charge density (in fraction of one electron) for the orbitals of a_{1g}, e_g and t_{2g} symmetry for $Fe(3d^6 4s^2)Ar_{12}$ Cluster.

ORBITAL	ORBITAL ENERGY (-Ry)	Charges in muffin-tin spheres			
		Fe	Ar	outer sphere	inter-atomic
$1a_{1g}\uparrow$(Ar3s)	1.800	0.0	0.995	0.0	0.005
$1a_{1g}\downarrow$(Ar3s)	1.800	0.0	0.995	0.0	0.005
$2a_{1g}\uparrow$(Ar3p)	0.794	0.024	0.942	0.002	0.032
$2a_{1g}\downarrow$(Ar3p)	0.792	0.017	0.950	0.002	0.031
$3a_{1g}\uparrow$(Fe4s)	0.421	0.787	0.089	0.001	0.123
$3a_{1g}\downarrow$(Fe4s)	0.337	0.737	0.105	0.002	0.156
$1e_g\uparrow$(Ar3s)	1.772	0.0	0.998	0.0	0.002
$1e_g\downarrow$(Ar3s)	1.772	0.0	0.998	0.0	0.002
$2e_g\uparrow$(Ar3p)	0.783	0.019	0.951	0.001	0.029
$2e_g\downarrow$(Ar3p)	0.783	0.001	0.969	0.001	0.029
$3e_g\uparrow$(Ar3p)	0.758	0.052	0.932	0.003	0.013
$3e_g\downarrow$(Ar3p)	0.757	0.001	0.983	0.004	0.012
$4e_g\uparrow$(Fe3d)	0.733	0.924	0.072	0.0	0.004
$4e_g\downarrow$(Fe3d)	0.410	0.985	0.003	0.0	0.012
$1t_{2g}\uparrow$(Ar3s)	1.775	0.0	0.997	0.0	0.003
$1t_{2g}\downarrow$(Ar3s)	1.775	0.0	0.997	0.0	0.003
$2t_{2g}\uparrow$(Ar3p)	0.789	0.023	0.949	0.001	0.027
$2t_{2g}\downarrow$(Ar3p)	0.788	0.001	0.971	0.001	0.027
$3t_{2g}\uparrow$(Ar3p)	0.765	0.063	0.918	0.002	0.017
$3t_{2g}\downarrow$(Ar3p)	0.763	0.002	0.979	0.003	0.016
$4t_{2g}\uparrow$(Fe3d)	0.732	0.912	0.085	0.0	0.003
$4t_{2g}\downarrow$(Fe3d)	0.410	0.985	0.005	0.0	0.010

TABLE III

Electron charge densities (in atomic units) at the Fe nucleus for $FeAr_{12}$ clusters and Fe atom. $\Delta\rho(0)$ values are relative to the free atom.

ORBITAL	$Fe(3d^64s^2)Ar_{12}$	$Fe(3d^64s^1)Ar_{12}^+$	$Fe(3d^74s^1)Ar_{12}$	$Fe3d^64s^2$
Fe↑1s	5376.081	5375.990	5376.990	5375.904
Fe↓1s	5376.143	5376.032	5376.115	5375.962
Fe↑2s	488.566	488.578	488.889	488.528
Fe↓2s	490.319	490.363	490.175	490.358
Fe↑3s	71.257	72.198	70.507	71.277
Fe↓3s	70.426	70.420	69.996	70.439
$1a_{1g}$↑(Ar3s)	0.0	0.0	0.0	-
$1a_{1g}$↓(Ar3s)	0.0	0.0	0.0	-
$2a_{1g}$↑(Ar3p)	0.101	0.746	0.063	-
$2a_{1g}$↓(Ar3p)	0.057	0.101	0.027	-
$3a_{1g}$↑(Fe4s)	5.615	6.088	4.770	5.084
$3a_{1g}$↓(Fe4s)	4.598	-	-	3.839
total	11883.163	11880.516	11876.657	11881.391
$\Delta\rho(0)$	+ 1.77	- 0.88	- 4.73	

FIGURE CAPTIONS

Figure 1 - Energy level spectra for the $Fe(3d^6 4s^2)Ar_{12}$ and $ArAr_{12}$ clusters. The energies are refered to the HOMO level in the Ar3p band (t_{1g}) which has been taken as the zero of the scale.

Figure 2 - Energy level spectrum for the $Fe(3d^7 4s^1)Ar_{12}$ cluster.

Figure 3 - Energy level spectrum for the $Fe(3d^6 4s^1)Ar_{12}^+$ cluster.

Figure 4 - Radial charge distributions for the $a_{1g}\uparrow$(Fe4s) orbital in $Fe(3d^6 4s^2)Ar_{12}$ and the 4s↑ free atom function.

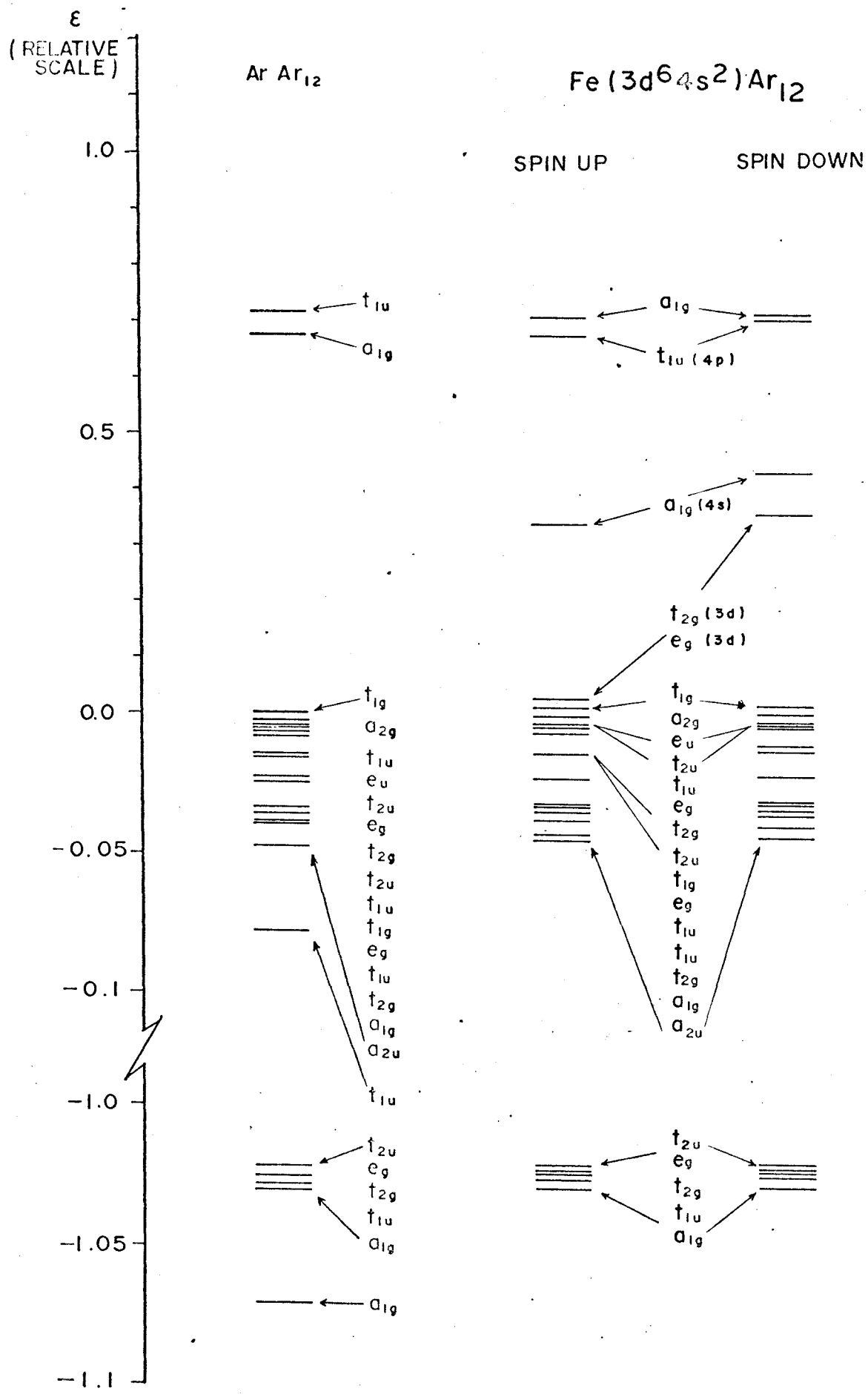
ε
(RELATIVE SCALE)
1.0
0.5
0.0
-0.05
-0.1
-1.0
-1.05
-1.1
Ar Ar12
Fe(3d64s2)Ar12
SPIN UP
SPIN DOWN
t1u
a1g
t1g
a2g
t1u
eu
t2u
eg
t2g
t2u
t1u
t1g
eg
t1u
t2g
a1g
a2u
t1u
t2u
eg
t2g
t1u
a1g
a1g
t1u (4p)
a1g (4s)
t2g (3d)
eg (3d)
t1g
a2g
eu
t2u
t1u
eg
t2g
t2u
t1g
eg
t1u
t1u
t2g
a1g
a2u
t2u
eg
t2g
t1u
a1g

Figure 1

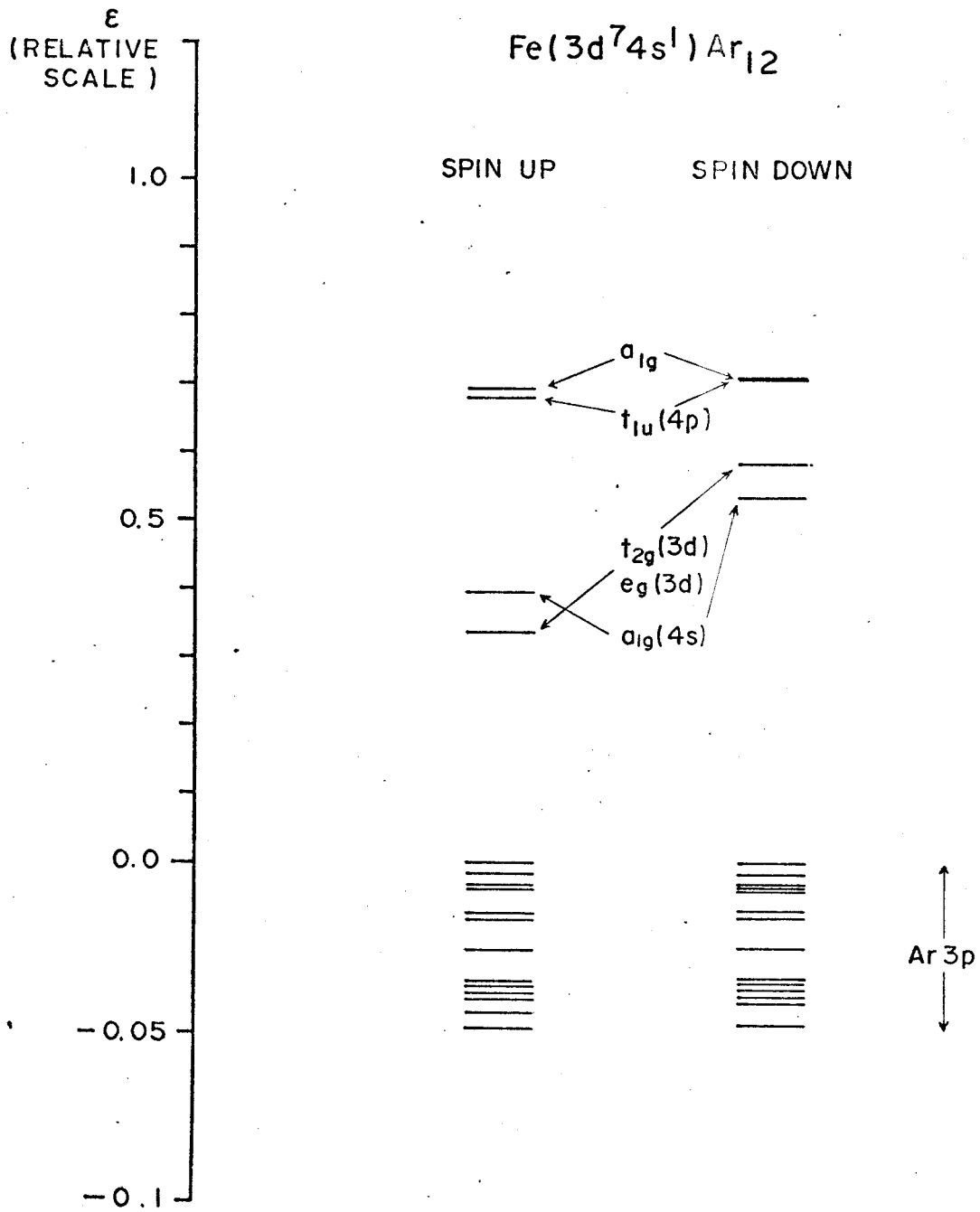
ε
(RELATIVE
SCALE)
1.0
0.5
0.0
−0.05
−0.1
Fe(3d⁷4s¹)Ar₁₂
SPIN UP
SPIN DOWN
a1g
t1u(4p)
t2g(3d)
eg(3d)
a1g(4s)
Ar 3p

Figure 2

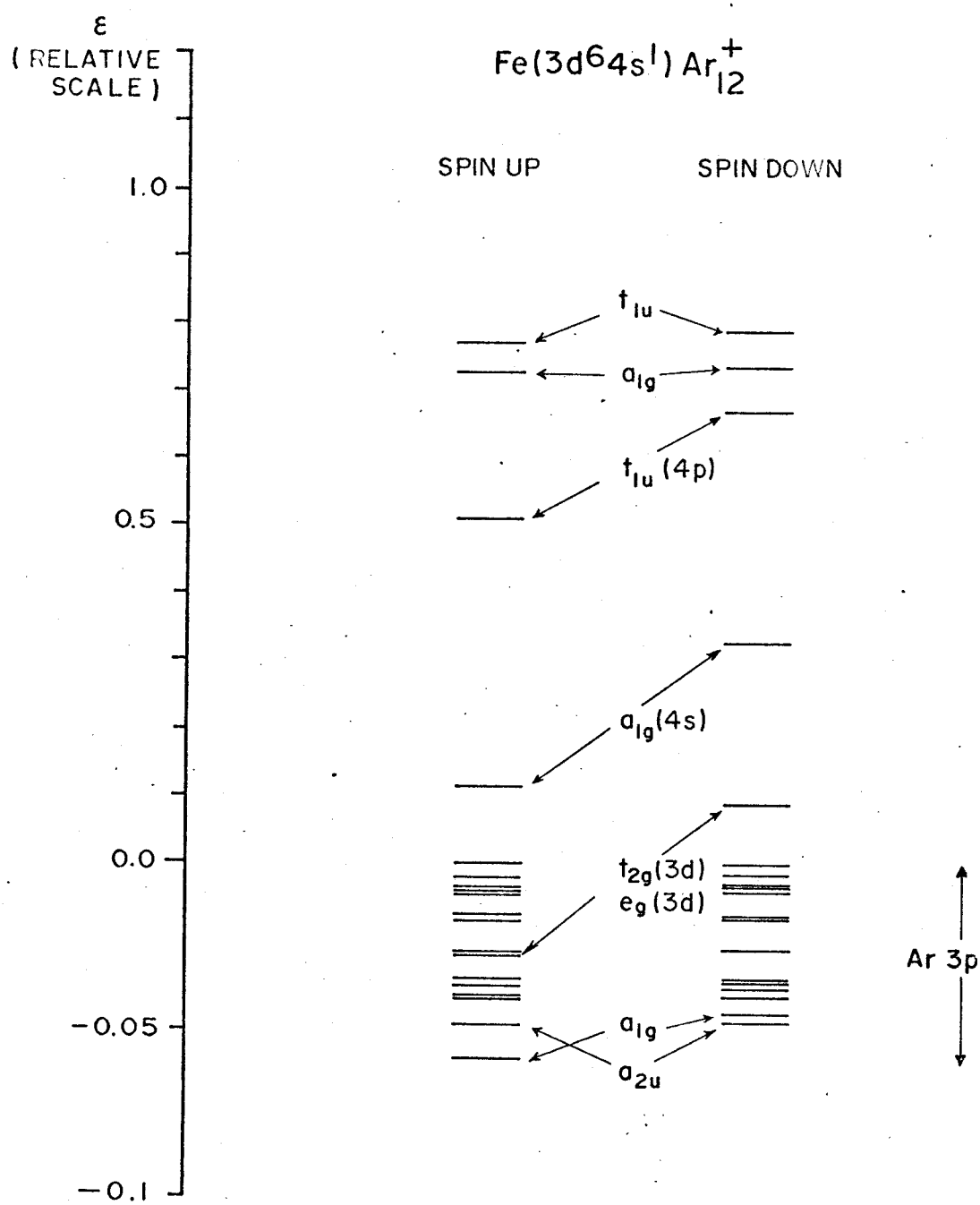
ε
(RELATIVE SCALE)
1.0
0.5
0.0
−0.05
−0.1
Fe(3d64s1) Ar12+
SPIN UP
SPIN DOWN
t1u
a1g
t1u (4p)
a1g(4s)
t2g(3d)
eg(3d)
a1g
a2u
Ar 3p

Figure 3

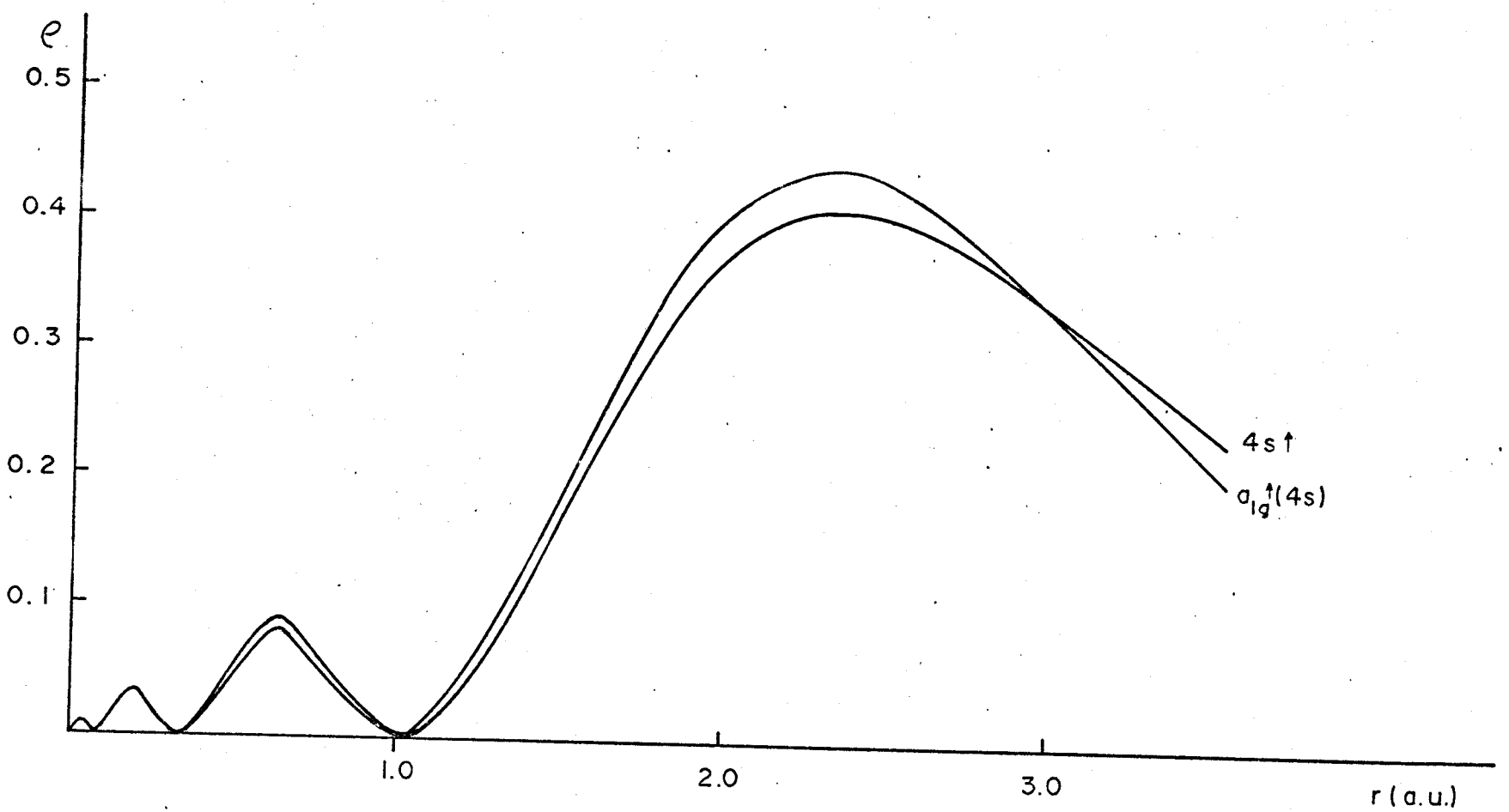

Figure 4